

Characterization by Fourier Transform Infrared Spectroscopy (FT-IR) and 2D IR Correlation Spectroscopy of PAMAM Dendrimer

Maria-Cristina Popescu,^{*,†} Daniela Filip,^{‡,§} Cornelia Vasile,^{*,†} C. Cruz,^{§,||} J. M. Rueff,[⊥] Mercedes Marcos,[⊥] J. L. Serrano,[⊥] and Gh. Singurel[#]

“Petru Poni” Institute of Macromolecular Chemistry, 41 A Alley Gr. Ghica Voda, 700487-Iasi, Romania, Department de Materiais, FCT/UNL and CENIMAT, Quinta da Torre, 2829-516 Caparica, Portugal, Centro de Física da Matéria Condensada da Universidade de Lisboa, Av. Prof. Gama Pinto 2, 1649-003 Lisboa, Portugal, IST-UTL, Av. Rovisco Pais 1049-001 Lisboa, Portugal, Química Orgánica, Facultad de Ciencias-ICMA, Universidad de Zaragoza-CSIC, E-50009 Zaragoza, Spain, and Spectroscopy Laboratory, “Al. I. Cuza” University, 11 Bd Carol I, Iasi, Romania

Received: March 2, 2006; In Final Form: May 29, 2006

FT-IR and 2D correlation spectroscopy were employed to study the microstructural changes occurring during phase transitions of a liquid crystal poly(amidoamine) codendrimer (PAMAM (L₁)₁₆(L₂)₁₆) generation 3, functionalized on the terminal groups by one-chain promesogenic calamitic units (4-(4'-decyloxybenzoyloxy)-salicylaldehyde (L₁)) and two-chain promesogenic calamitic units (4-(3',4'-didecyloxybenzoyloxy)salicylaldehyde (L₂)). Spectral modifications associated with molecular conformation rearrangements allowing for molecular shape change on going from a liquid–crystalline organization to another were found. The transition temperatures were calculated, and they are in good agreement with the DSC data. Spectral analysis gives evidence of the LC phase transitions and to an additional transition associated with the existence of conformers. Various types of hydrogen bonding have been established.

Introduction

Dendrimers are polymeric three-dimensional macromolecules. Branched molecular architecture imparts their particular physicochemical properties, such as high solubility,¹ low viscosity in solution² and melt, absence of entanglements, low glass transition values,³ and a capacity to act as dendritic boxes, i.e., to encapsulate certain molecules.⁴ Numerous dendritic structures have been synthesized and studied, including polyamidoamines,⁵ polyamides,⁶ polyphenyl ethers,¹ carbosilanes,⁷ etc. The study of dendrimers with different functionalities is particularly interesting due to their unique superbranched architecture, high density of peripheral functionalities, symmetrical shape, and monodispersity. Such compounds have units capable of performing specific functions, such as electron-transfer processes (transition-metal units⁸), antenna effects (different chromophoric groups⁹), photoinduced processes (photoisomerizable groups^{10,11}), etc. The achievements in this promising field concerning the synthesis and relationship between the molecular structure and properties of dendrimers have been published in numerous publications, reviews,^{12–14} and in a monograph.⁶ Dendrimers containing mesogenic groups can also display liquid–crystalline (LC) phases.^{15–18} LC dendrimers have attracted considerable attention from researchers working both in the areas of polymers and low-molar-mass liquid crystals. A comprehensive review on LC dendrimers was published in ref 12.

In view of constructing tailored functional nanomaterials and to determine the structural criteria involved in their self-assembling and self-organization processes, new poly(amidoamine) (PAMAM) and poly(propyleneimine) (DAB)^{19–22} end-functionalized dendromesogens were synthesized and characterized. These liquid–crystalline dendrimers are obtained by attaching promesogenic units to the termini of the preexisting dendrimer core (PAMAM or DAB), up to the fifth generation. Crucial in the LC organization of these compounds is the competition between two opposite tendencies within the same molecule: the tendency to the isotropic distribution in space of the dendritic branches resulting in spherical morphology (starburst shape) due to entropic forces and the strong interactions between the terminal mesogenic groups which preferentially favor anisotropic order driven by the enthalpic gain. Due to the chemical incompatibility between the dendritic core and the functionalized terminal mesogenic, promesogenic, or nonmesogenic groups, a microphase separation occurs at the molecular level, and these dendromesogens could be regarded as block copolymers. Mesomorphism could be strongly improved by the layering of the system. Microphase segregation constitutes an important driving force in mesophase formation. Two possible molecular conformations of the dendromesogens are responsible for the mesophase formation:

In the case of the parallel model responsible for smectic organization, the mesogenic units are arranged parallel to one another, and the dendritic molecule is constrained to fit to the anisotropic environment and therefore must be soft enough to adapt to an anisotropic shape of a cylindrical object. In the smectic phase the mesogenic units are extending up and down from the molecule center. The layering ordering of these diblock rods is enhanced by the amphipathic character of the molecule.

In the case of the radial model, the mesogenic units are

* Corresponding authors e-mail: cvasile@mail.icmpp.ro (C.V.) and cpopescu@mail.icmpp.ro (M.-C.P.).

[†] “Petru Poni” Institute of Macromolecular Chemistry.

[‡] FCT/UNL and CENIMAT.

[§] Centro de Física da Matéria Condensada da Universidade de Lisboa.

^{||} IST-UTL.

[⊥] Universidad de Zaragoza-CSIC.

[#] “Al. I. Cuza” University.

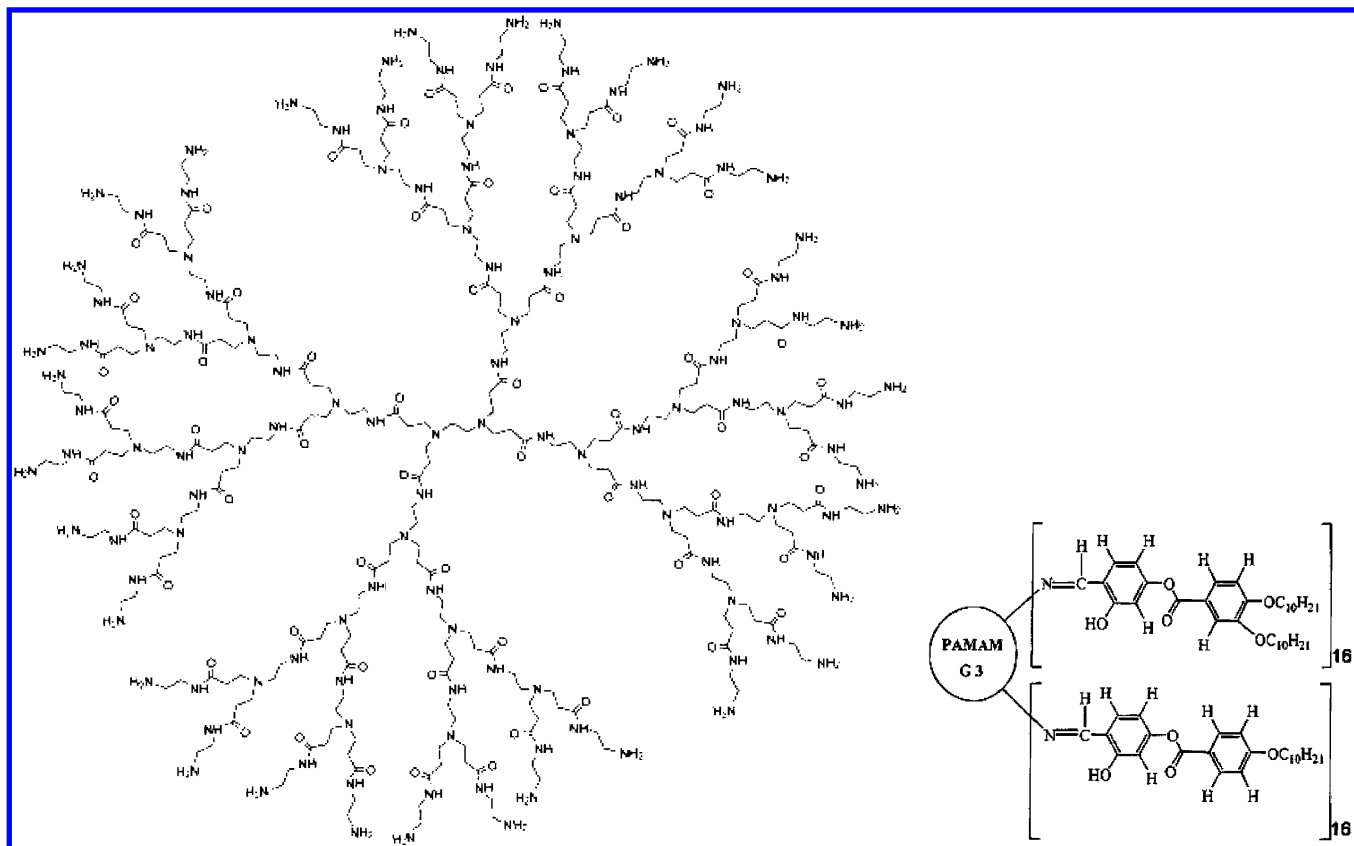


Figure 1. Structure of the PAMAM dendrimer.

disposed radially around a central moiety inducing columnar mesomorphism. The formation of this radially layered structure of the block dendrimers is driven by microphase separation between the incompatible segments of the molecule.

By changing the molecular shape of these supermolecules different types of LC organization are obtained.

For the PAMAM dendromesogens²³ it was found that one aliphatic terminal chain per mesogenic group favors their parallel arrangement, while on increasing the aliphatic chain density the promesogenic units are forced to be radially arranged and columnar mesophases are formed.²³ This was explained by the modification of aliphatic/aromatic interfacial curvature. Therefore the thermotropic mesophases are affected by molecular curvature in the same way as the curvature affects lyotropic systems.

To obtain new dendrimer molecules which could exhibit a transformation from lamellar to columnar mesophase within the same compound, PAMAM liquid-crystalline codendrimers functionalized by two different promesogenic units bearing one or two terminal aliphatic chains, respectively, have been synthesized and characterized.²² By modifying the comonomer ratio and the density of aliphatic chains at the outer surface of the dendrimers a change from smectic to columnar mesophase was observed. Moreover a columnar rectangular phase was obtained. This result constitutes the strong evidence of changing of the molecular shape from oblate to prolate in the transition from lamellar to columnar phase.

The codendrimer taken in the present study belongs to this series of compounds.²² The structure and the phase transitions are presented in Figure 1. It is characterized by a columnar rectangular and smectic A liquid-crystalline phases and presents the $g \rightarrow Col_r \rightarrow Sm A \rightarrow I$ phase sequence with increasing temperature.

The physical and electro-optical properties of this type of compounds are strongly dependent on their molecular shape and local environments. The molecules forming liquid crystals have a variety of conformational and orientational states with statistical distribution and equilibrium population of several possible molecular conformations. However, the relationship between molecular structure and arrangement in each phase has not been clearly elucidated.

IR spectroscopy is a well-established nondestructive method for highly sensitive and selective concentration determination and identification of chemical species. The specific absorption of the substance in the "fingerprint" region enables the distinct recognition of various chemical species and even of structural isomers. Vibrational frequencies are very sensitive to small changes in the bonding and geometrical arrangement of atoms in molecules. Infrared spectroscopy provides direct and distinct information about the molecular structure, conformation, and orientation of individual segments of LC molecules.^{24,25} Fourier transform infrared (FT-IR) spectroscopy offers the accessibility to H-bond interactions in these systems, real-time conformational and structural changes during temperature variations,^{26,27} and orientational behavior. The development of the two-dimensional-2D correlation spectroscopy opened new possibilities in this field. This new technique is a more powerful tool for studying spectral changes induced by external perturbation. Two-dimensional (2D) correlation spectroscopy is a mathematical tool whose basic principles were first laid down by Noda.²⁸ A simple cross-correlation analysis was applied to sinusoidal varying dynamic IR signals to construct a set of 2D IR correlation spectra.²⁹ Generalized 2D correlation spectroscopy, which is an extension of original 2D correlation spectroscopy, allows for the application of a variety of perturbations to generate 2D correlation spectra of the analyzed system.²⁹ In generalized 2D correlation spectroscopy, the change in the

spectra alteration can be monitored as a function of any physical or chemical variable, as e.g. time,³⁰ temperature,³¹ pressure,³² or concentration,³³ among others. Following the pioneering work of Noda, many research groups have adopted 2D correlation analysis to study e.g. self-associated molecules,³⁴ polymers,³⁵ and biological molecules, such as peptides³⁶ and proteins.³⁷

By spreading peaks along the second dimension, 2D correlation spectroscopy sort out complex or overlapped spectral feature and enhances spectral resolution.³⁸ Additional useful information can be extracted which cannot be obtained straight from the conventional one-dimensional spectra or only by means of 2D correlation spectroscopy, because it reflects the response of the system to the external perturbation. Correlation between changes at different spectral positions can be obtained. If overlapping subcomponents of a complex band reply to the external perturbation in different ways, resolution enhancement can also be achieved. These features allow a detailed investigation of the effect of the perturbing parameter on inter- as well as on the intramolecular interactions.

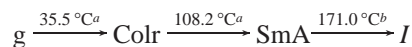
In the last 10 years the FT-IR spectroscopy and especially 2D correlation spectroscopy proved to be very powerful techniques for the study of the structural modifications of the liquid-crystalline substances and their transitions phenomena during heating and cooling.^{39–44}

In the present study, a liquid crystal poly(amidoamine) codendrimer (PAMAM (L₁)₁₆(L₂)₁₆ generation 3, functionalized in the terminal groups by one-chain promesogenic calamitic units (4-(4'-decyloxybenzoyloxy)salicylaldehyde (L₁)) and two-chain promesogenic calamitic units (4-(3',4'-didecyloxybenzoyloxy)salicylaldehyde (L₂)),²² is investigated by FT-IR and 2D correlation spectroscopy. The sequential order of changes in the molecular environment and conformations of the functional groups during LC phase transitions is evidenced.

Experimental Section

Materials. The synthesis and characterization of the liquid-crystalline poly(amidoamine) codendrimer (PAMAM (L₁)₁₆(L₂)₁₆ generation 3, functionalized in the terminal groups by one-chain promesogenic calamitic units (4-(4'-decyloxybenzoyloxy)salicylaldehyde (L₁)) and two-chain promesogenic calamitic units (4-(3',4'-didecyloxybenzoyloxy)salicylaldehyde (L₂)), are reported in ref 22. It has been synthesized at the University of Zaragoza. The dendrimer exhibit columnar-rectangular and smectic A phase. The structure of the PAMAM dendrimer generation 3 and of the corresponding LC codendrimer along with the phase sequence is represented in Figure 1.

Phase sequence by heating of the PAMAM (L₁)₁₆(L₂)₁₆ codendrimer detected by DSC is the following



where *a* is the second heating scan without reaching the isotropic temperature, and *b* is the first heating scan of a different sample reaching the isotropic temperature.

The changes during heating/cooling can be explained taking into account the following considerations about possible textures of the phases. The space available for the dendritic core in the smectic mesophase is easy to estimate by simple calculations based on the measured layer thickness. The volume of a dendrimer molecule can be estimated from the molecular mass and the density. Then, the molecular cross-section area in Å² can be expressed as $\text{Area} = V/d$, where *V* is the molecular volume and *d* is the layer thickness in the smectic mesophase

(57 Å in this case). Assuming that the density must be close to 0.9 g cm⁻³, the calculated molecular area is about 700 Å². As the molar mass of the dendritic core (6909) is 32% of the total molar mass (21 584), this implies that the thickness of the sublayer occupied by the core should be $57 \times 0.32 = 18.2 \text{ Å}^2$, which is reasonable assuming that the terminal hydrocarbon chains are disordered. The volume available for the core is about $700 \times 18.2 = 12\,740 \text{ Å}^3$. This is enough space to accommodate a mass of 6909 with a density of about 0.9 g cm⁻³, obviously in a very disordered conformational state. Furthermore, as the molecule contains a total number of 48 terminal hydrocarbon chains which statistically extend upward and downward from the central core, the cross-section area available for each chain is $700/24 = 29 \text{ Å}^2$, a reasonable value for a molten hydrocarbon chain.

The samples were characterized by FT-IR spectroscopy coupled with 2D correlation spectroscopy. FT-IR spectra were recorded on heating to 130 °C followed by cooling to room temperature, using a heating/cooling rate of 1 °C/min.

Investigation Methods

FT-IR Spectroscopy. FT-IR spectra at different temperatures were recorded on solid sample in KBr pellet by means of a FT-IR DIGILAB, Scimitar Series Spectrometer (U.S.A.) with a resolution of 4 cm⁻¹. The concentration of the sample in pellets was 3 mg/500 mg KBr. The phase behavior of the sample was followed both on heating and on cooling using a heating/cooling rate of 1 °C/min. The maximum temperature of heating was 130 °C, below the degradation of the sample which takes place at about 170 °C. The results are the average of the three successive determinations. Processing of the spectra was done by means of Grams/32 program (Galactic Industry Corporation). The reduced χ^2 for all deconvoluted and fitted curves was $\chi^2 < 0.01$. The second derivative of the IR spectra was obtained with the Savitsky-Golay method (second-order polynomial with 15 data points) using Grams 32 program.

2D Correlation Spectroscopy. 2D FTIR correlation intensities were calculated using our own Matlab program using the generalized 2D correlation method developed by Noda.²⁸ For all calculations, the spectrum recorded at room temperature was used as the reference spectrum. In 2D correlation analysis, two kinds of correlation maps synchronous and asynchronous are generated from a set of dynamic spectra obtained from the modulation experiment.²⁹ Synchronous 2D-correlation spectra represent the simultaneous or coincidental changes of spectral intensities measured at the wavenumbers ν_1 and ν_2 . Correlation peaks appearing at the diagonal position ($\nu_1 = \nu_2$) correspond to the linear evolution of a given species along the induced perturbation. However, such a correlation peak does not provide major information since its intensity value only depends on change in single absorbance band intensity. Thus, such a correlation peak is considered as an autopeak.⁴⁵ On the other hand, correlation peaks appearing out of the diagonal position ($\nu_1 \neq \nu_2$) correspond to the simultaneous changes of spectral signals at two different wavenumbers, which may be positively correlated (the two signals evolve correlatively in the same direction) or negatively correlated (the two signals evolve correlatively in opposite directions) with each other. The asynchronous 2D correlation spectra represent sequential, or unsynchronized, changes of spectral intensities at the wavenumbers ν_1 and ν_2 . The spectrum is antisymmetric with respect to the diagonal line, and, thus, correlation peaks only appear out of the diagonal line. An asynchronous correlation peak develops only if the intensities of the two dynamic spectral

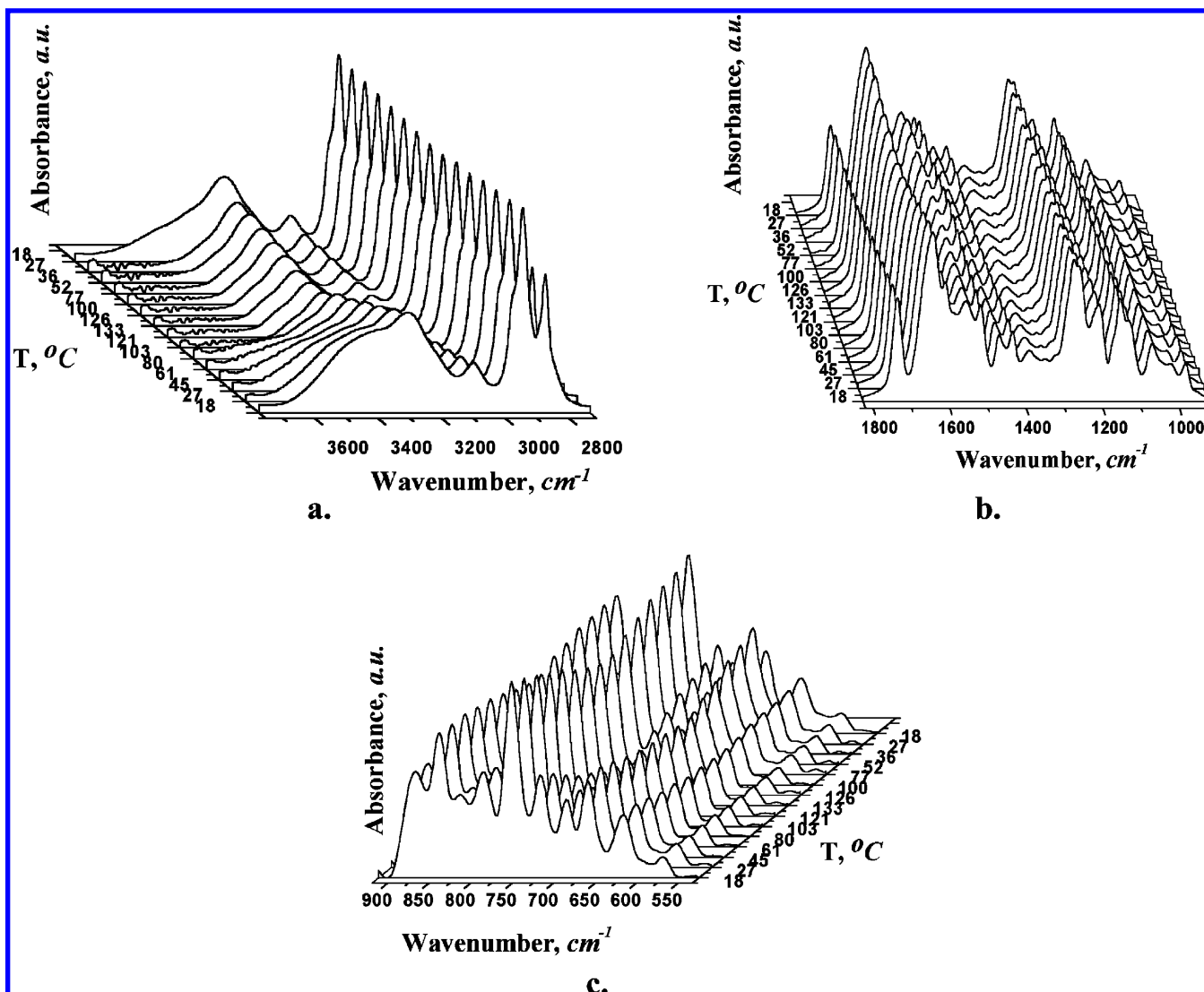


Figure 2. 3D representation of the spectral modifications in the following spectral regions: 2700–3800 cm^{-1} (a), 1000–1800 cm^{-1} (b), and 600–1000 cm^{-1} (c).

intensities vary out of phase (delayed or accelerated) with each other. The sign of an asynchronous correlation peak may be positive if the intensity change at ν_1 occurs predominantly before ν_2 , or it may be negative if the change occurs after ν_2 . According to Noda,²⁹ the sign of asynchronous peaks provides very useful information about the temporal sequence of events taking place during the studied process.

With combined synchronous spectra and asynchronous spectra generated during heating, the variation sequence of different groups could be estimated. The rules are as follows: if the crosspeaks in the synchronous spectrum (ν_1 , ν_2) are positive (assume that $\nu_1 > \nu_2$), and the crosspeak at the same position in the asynchronous spectrum is also positive, then the change at ν_1 may occur prior to that of ν_2 . If the crosspeak in the asynchronous spectrum is negative, then the change at ν_2 may occur prior to that of ν_1 . If the ν_1 , ν_2 in the synchronous spectra is negative, then the rules are reversed.

Results and Discussion

Spectral modifications which occurred on heating and cooling processes of the sample are evidenced by 3D representations of the spectra. A detailed examination of them reveals modifications which occurred in the 2700–3800 cm^{-1} , 1000–1800 cm^{-1} , and 600–1000 cm^{-1} spectral regions (Figure 2 a, b, and

c, respectively). The band assignments and observations on modifications which occurred with temperature are presented in Table 1.

On cooling the sample down to room-temperature both the bands' location and their intensity are recovering.

The changes which occurred in the spectra could be due to the conformational and/or structural modifications or to phase transitions. The different sensitivity with temperature of the functional groups is put into evidence by plotting the integral absorption versus temperature. A detailed analysis of some of these dependencies is presented in Figure 3. It can be noticed for all the spectral regions that the integral absorption decreases with increasing temperature. On cooling the process is reversed, for all bands, a longer time (>24 h) interval being necessary for the bands in the 1090–1180 cm^{-1} region.

In the 3130–3700 cm^{-1} spectral region (Figure 3a), corresponding to O–H and N–H stretching it is evidenced a change at ≈ 45 °C; in the 1180–1330 cm^{-1} spectral region (Figure 3b) it is evidenced a change at ≈ 120 °C, whereas in the region 1090–1180 cm^{-1} (Figure 3c) changes can be observed at ≈ 45 °C, at ≈ 95 °C, and at ≈ 120 °C (arrows on figures).

The most sensitive band to the temperature variation is that at 3470 cm^{-1} corresponding to free OH groups. This band

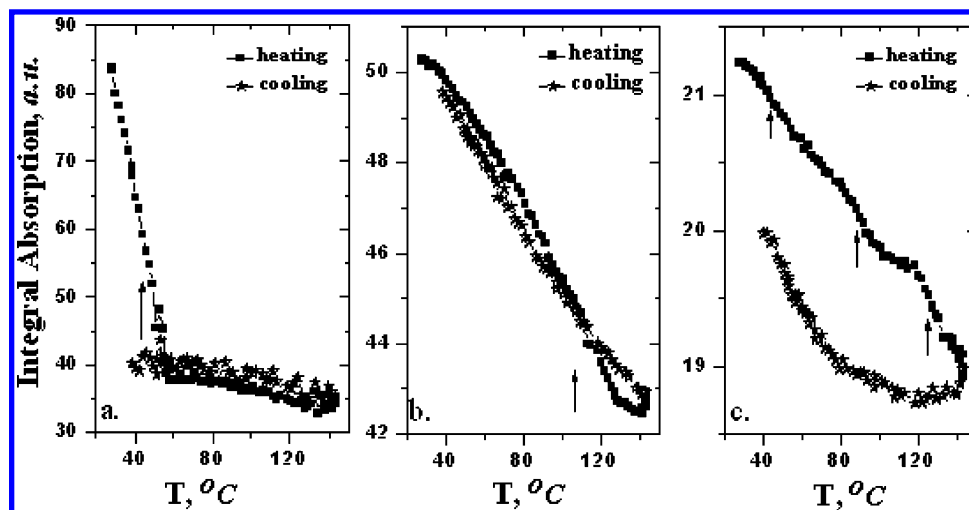


Figure 3. The variation of the integral absorbance as a function of temperature for 3130–3700 cm^{-1} (a), 1180–1330 cm^{-1} (b), and 1090–1180 cm^{-1} (c).

TABLE 1: Band Assignments and Observations on Modifications Occurred with Temperature

band position (cm^{-1})	assignment	observations on bands modification
3470	stretching vibration of free OH groups	vanishes during sample heating and reappears on cooling but with a lower intensity
3395	stretching vibrations of H-bonded OH groups	slight decrease during heating
3285	stretching vibrations of free NH groups	slight shift to high wavenumbers and a slight decrease in intensity
3190	stretching vibrations of H-bonded N–H groups	slight decreases of intensity during heating are recovered during cooling
3078	aromatic C–H stretch	
2952	stretching vibrations of aliphatic groups	
2924	stretching vibrations of aliphatic groups	
2854	stretching vibrations of aliphatic groups	stretching vibrations of aliphatic groups
1729	stretching vibrations of ester C=O groups	is shifted at 1736 cm^{-1} slight decrease in intensity during heating
1657	amide I mode	slight increase in intensity and is shift toward high wavenumbers 1661 cm^{-1}
1631	CH=N groups	slight decreases in intensity
1605	C=C from aromatic ring	
1580	C=C from aromatic ring	
1430	stretching vibrations of C–H groups from aromatic ring	stretching vibrations of C–H groups from aromatic ring
1532	amide II	slight decrease and a shift to low wavenumber 1539 cm^{-1}
1270	stretching vibrations of C–O–C groups	slight shift to low wavenumbers and a decrease in intensity
1256	C–O stretching or CNH (amide III)	slight decreases in intensity
1214	C–H bending mode	
1204	C–N stretching vibration	
1150	C–N stretching vibration	
1126	aromatic ring vibrations	aromatic ring vibrations

vanishes on heating at ≈ 50 $^{\circ}\text{C}$ and reappears on cooling at ≈ 30 $^{\circ}\text{C}$ but with a lower intensity (not plotted separately).

To make these spectral modifications clearer the spectra were deconvoluted with Gaussian type function, and the variations with temperature of integral absorption, wavenumber shift, and spectral width are plotted.

The modifications in PAMAM bands position and the deconvolution of the complex spectral region in component bands were realized in accordingly with the second derivative method. Generally, the secondary derivative IR spectra can obviously enhance the apparent resolution and amplify tiny differences of IR spectrum. The frequencies appearing in Table 2 come from the second derivative method.

Therefore, for the spectrum recorded at room temperature (Figure 4a), the region 3130–3700 cm^{-1} including the free and bonded absorptions of the OH and NH groups is resolved in four bands: the first one at 3470 cm^{-1} corresponding to the stretching vibrations of free OH groups, the second at 3395 cm^{-1} corresponding to stretching vibrations of H-bonded OH groups, the third at 3285 cm^{-1} , and the fourth at 3190 cm^{-1} corresponding to free N–H groups and H-bonded N–H groups, respectively. The OH band is recognizable by its broadness and

low intensity. For the spectrum recorded at 130 $^{\circ}\text{C}$ (Figure 4b), this region is resolved only in three bands because the band at 3470 cm^{-1} vanishes after ≈ 50 $^{\circ}\text{C}$.

The OH groups are present only in the terminal promesogenic units and ensure intramolecular H bonding which favor spatial arrangements for strong anisotropic interaction forces and packing, contributing to the stabilization of the LC phase. The amide groups are present only in the dendritic core. The intra- and intermolecular hydrogen bonds between them assures the stability of the central structure.

Using the value from wavenumber corresponding to the maximum of absorption bands of hydrogen bonds, the energy and hydrogen bonding distance can be estimated. The results are presented in Table 2.

The energy of the hydrogen bonds has been evaluated using the following formulas⁴⁶

$$E_{\text{H}} = \frac{1}{k} \left[\frac{(\nu_0 - \nu)}{\nu_0} \right]$$

where ν_0 is the standard frequency of the OH (3650 cm^{-1}) and NH (3474 cm^{-1}) monomers observed in the gas phase while ν

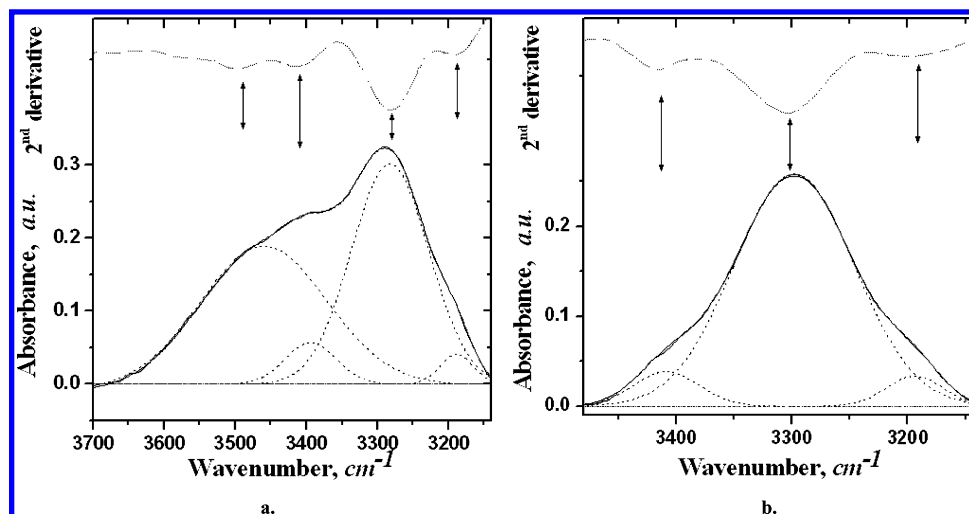


Figure 4. Deconvolutions of PAMAM spectra in the 3700–3100 cm^{-1} region at 18 °C (a) and 130 °C (b).

TABLE 2: Hydrogen Bonding Distance and the Energy of the Hydrogen Bonds at Heating and Cooling for OH and NH Groups

$T, ^\circ\text{C}$	ν, cm^{-1}	E, kJ	ν, cm^{-1}	E, kJ	ν, cm^{-1}	E, kJ	$R, \text{\AA}$	ν, cm^{-1}	E, kJ	$R, \text{\AA}$
20	3455	14.01	3385	19.02	3281	14.57	2.85	3188	21.65	2.68
30	3463	13.44	3395	18.34	3283	14.43	2.86	3189	21.55	2.69
40	3480	12.18	3398	18.12	3285	14.27	2.86	3190	21.45	2.69
50	3493	11.32	3407	17.50	3290	13.88	2.88	3191	21.36	2.69
60			3408	17.44	3293	13.66	2.88	3192	21.31	2.69
70			3408	17.394	3296	13.43	2.89	3193	21.26	2.70
80			3408	17.384	3298	13.30	2.89	3193	21.23	2.70
90			3409	17.34	3300	13.15	2.89	3193	21.23	2.70
100			3412	17.144	3302	13.02	2.89	3193	21.20	2.70
110			3412	17.08	3303	12.89	2.90	3194	21.17	2.70
120			3414	16.96	3306	12.72	2.90	3194	21.13	2.70
130			3415	16.91	3307	12.65	2.90	3196	21.04	2.70
120			3413	17.02	3306	12.68	2.90	3195	21.06	2.70
110			3412	17.09	3306	12.71	2.90	3195	21.08	2.70
100			3411	17.20	3305	12.75	2.90	3195	21.09	2.70
90			3410	17.25	3305	12.78	2.90	3195	21.10	2.70
80			3409	17.34	3304	12.83	2.90	3195	21.12	2.70
70			3407	17.47	3303	12.88	2.89	3194	21.13	2.70
60			3406	17.55	3303	12.92	2.89	3194	21.14	2.70
50			3404	17.66	3298	13.29	2.88	3194	21.17	2.70
40			3403	17.77	3297	13.36	2.88	3189	21.52	2.69
30			3401	17.92	3293	13.69	2.87	3189	21.53	2.69
20	3460	13.68	3393	18.49	3291	13.84	2.87	3188	21.58	2.68

is the stretching frequency of OH and NH groups observed in the infrared spectrum of the sample, and k is a constant equal to $2.625 \times 10^2 \text{ kJ}$.

The hydrogen bonding distance are obtained by using the Sederholm equation,⁴⁷ namely

$$\Delta\nu(\text{cm}^{-1}) = 0.548 \cdot 10^3(3.21 - R)$$

where $\Delta\nu = \nu_0$ (stretching frequency of the NH monomer observed in gas phase) – ν (stretching frequency observed in the infrared spectrum of the sample), and ν (monomeric NH stretching frequency) is taken to be 3474 cm^{-1} .⁴⁷

It can be observed from the bands at $3455\text{--}3492 \text{ cm}^{-1}$ and $3385\text{--}3414 \text{ cm}^{-1}$ that the hydrogen bonding energy values on heating are $14.01\text{--}11.32 \text{ kJ}$ and $19.02\text{--}16.91 \text{ kJ}$ while on cooling are 13.68 and $16.91\text{--}18.49 \text{ kJ}$, respectively. The bands at $3281\text{--}3007 \text{ cm}^{-1}$ and $3188\text{--}3196 \text{ cm}^{-1}$ have the hydrogen bonding energy on heating $14.57\text{--}12.65 \text{ kcal}$ and $21.65\text{--}21.04 \text{ kJ}$ and on cooling $12.65\text{--}13.84$ and $21.04\text{--}21.58 \text{ kJ}$, respectively. The hydrogen bonding distance for those bands is $2.86\text{--}2.90 \text{ \AA}$ and $2.68\text{--}2.70 \text{ \AA}$ on heating and $2.90\text{--}2.87 \text{ \AA}$ and $2.70\text{--}2.68 \text{ \AA}$ on cooling.

The results show that the OH groups exist in two hydrogen bonding modes in solid glassy phase and only in one mode in columnar rectangular and smectic A phases. The two modes of hydrogen bonding present significant changes before first transition from solid glassy phase to the columnar rectangular LC phase. After that, the OH band, which remains in the spectrum presents small changes with increasing temperature in the columnar and smectic A phases. This indicates that the functional groups involved in H bonding would bond in liquid–crystalline phases in a more efficient manner when comparing with solid glassy phase. The small changes which occurred in columnar rectangular and Sm A phases suggest the role of H bonding in formation and stabilization of the LC phases.

In Figure 5 the dependencies on temperature of the wavenumber of the free and bonded vibration modes of OH at 3450 and 3385 cm^{-1} and NH at 3285 and 3189 cm^{-1} groups are presented. On heating, all of the bands show shifts to high wavenumbers, reflecting the changes in strength of the hydrogen bonds and phase structures. The bonded modes which show discontinuities in the trends seem to be more sensitive and more affected by the liquid–crystalline-phase transitions. On cooling the process is reversed.

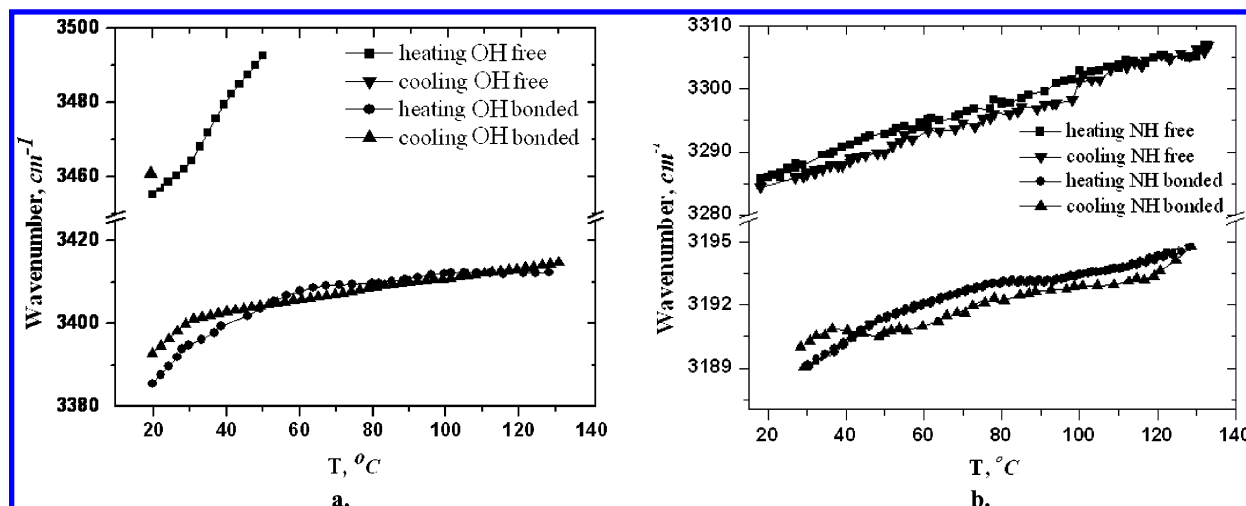


Figure 5. Dependencies on temperature of the wavenumber of the bands at 3450, 3385 cm^{-1} corresponding to the OH groups (a) and 3285, 3189 cm^{-1} corresponding to the NH groups (b).

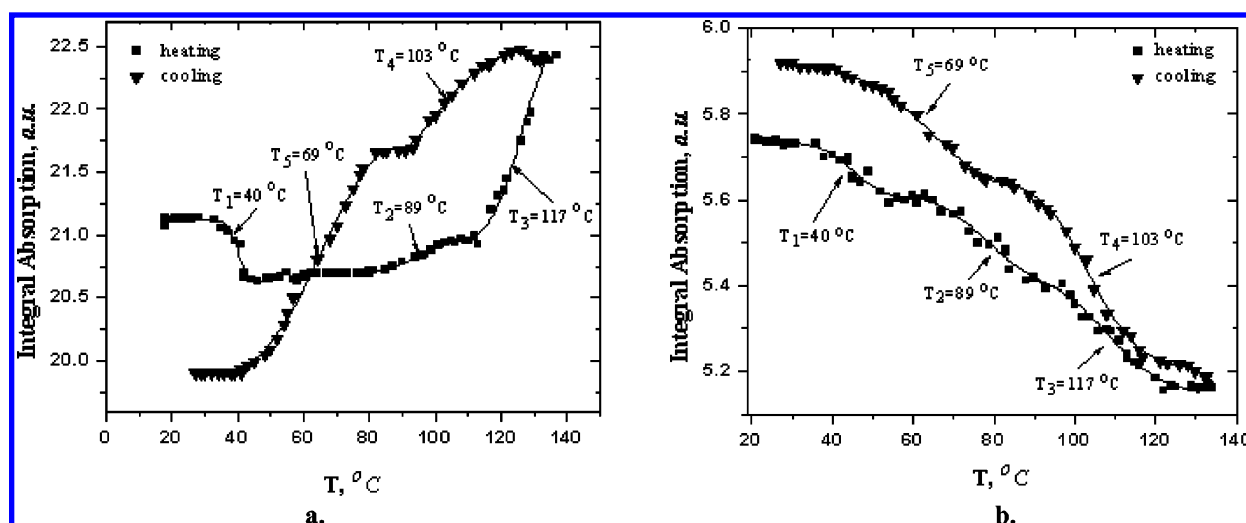


Figure 6. Dependencies on temperature of the integral absorption of the bands at 1657 cm^{-1} (a) and 1603 cm^{-1} (b).

In the regions 1800–1450 and 1330–1000 cm^{-1} significant variations with temperature are shown by the band at 1657 cm^{-1} (amide I mode) corresponding to the OC–NH group, present only in the dendrimeric core and the band at 1603 cm^{-1} corresponding to C=C from the aromatic ring present only in the promesogenic units. The dependencies on temperature of the integral absorption of these bands (obtained by deconvolution of spectra in these regions) are depicted in Figure 6.

By analyzing the two dependencies it can be noticed three changes on heating at ≈ 40 – 45°C , at ≈ 90 – 95°C , and at $\approx 120^\circ\text{C}$, whereas on cooling two changes at ≈ 100 – 105°C and at ≈ 67 – 70°C are observed.

For an accurate determination of the transition temperature, the curves of the dependence of integral absorption of these bands on temperature was fitted by Boltzmann functions (using Origin program) given by the following equation

$$y = \frac{A_1 - A_2}{1 + e^{\frac{(x - x_0)}{dx}}} + A_2$$

where A_1 is the minimum value of the function; A_2 is the maximum value of the function; x_0 is the value on the x axis corresponding to the inflection of the curve, equivalent to the transition temperature; and dx is the domain in which this value

is found. The reduced χ^2 for all the fitted curves was $\chi^2 < 0.1$; therefore, the use of this function is a good approach.

In Figure 6 the values of the integral absorbance at different temperatures of the bands at 1657 and 1603 cm^{-1} are represented by dots, with the solid line representing the Boltzmann fitted curve. By fitting procedure A_1 , A_2 , x_0 , and dx parameters are obtained. The value corresponding to x_0 is the value of the transition temperature.

The temperature values which resulted from the fitting process are $T_1 = 40^\circ\text{C}$, $T_2 = 89^\circ\text{C}$, and $T_3 = 117^\circ\text{C}$ on heating and $T_4 = 103^\circ\text{C}$ and $T_5 = 69^\circ\text{C}$ on cooling. The first and the last values agree very well with the DSC data.²² The second change at 89°C was not distinguished in the DSC curve as a phase transition. This phenomenon would be connected to an increased significance of temperature on rearrangements of molecular conformation with a change of the central dendritic conformation from a more pronounced prolate shape (disklike) characteristic to a columnar structure to a more pronounced oblate shape (ellipsoid) characteristic to a lamellar structure. On increasing temperature, H-bond breaking allows for the plastic dendritic molecule to become soft enough to fit to the anisotropic environment and to change its shape.

The abrupt changes revealed by the OC–NH groups which occurred at around 40 and 117°C and which can be associated with $g \rightarrow \text{Col}_r$ and $\text{Col}_r \rightarrow \text{Sm A}$ phase transitions reveal clearly

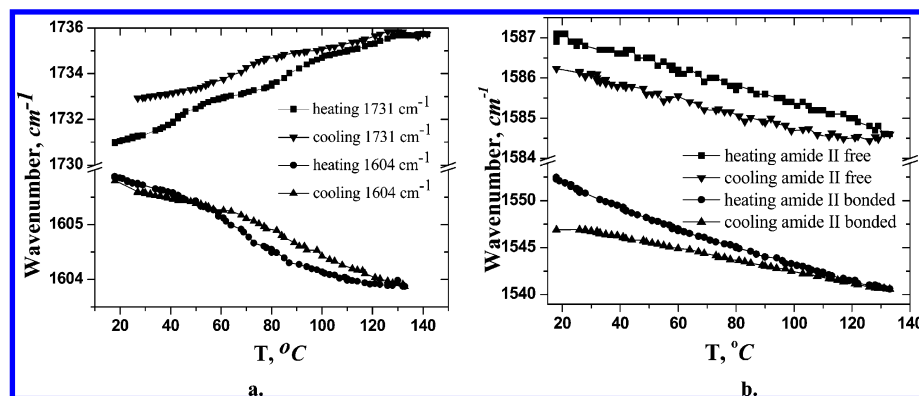


Figure 7. Temperature dependence of wavenumber of C=O and C=C vibrational bonds (a) and amide II bonds (b).

the contribution of the hydrogen bonds between the amide groups in preserving a rigid dendrimeric core necessary for the formation of the columnar mesophase. The transition from columnar to a higher temperature lamellar structure can be explained by destabilization of the aggregated central structure of the dendritic core through H-bond breaking. Therefore the achieved chain mobility and conformation freedom of the alkoxy chains and dendrimer core would favor layer segregation and formation of the Sm A phase.

Figure 7a gives the frequency changes of two vibrational modes the stretching mode of the ester C=O and aromatic C=C as a function of temperature. Each carbonyl group forms a π -electron resonance system with the neighboring phenyl ring.⁴³ The wavenumber shift with an external field indicates the changes in the interaction forces and molecular orientation.⁴⁸ As the temperature increases, the molecular structure changing from a solid glassy state to a columnar state and a smectic state, the interaction forces of inter- and intramolecular nature are reduced so the rotation freedom degree of the carbonyl group also increases and causes a reduction of resonance magnitude. Due to this factor, the frequency of the C=O band shifts to a higher wavenumber, while the frequency of the C=C stretching mode in aromatic rings changes in the reverse direction.

Figure 7b give the frequency changes of two vibrational modes assigned to the stretching mode of the free and bonded amide II. Contrary to the trend shown by the N-H stretching region, on heating a continuous shift to low wavenumbers of both amide II modes is observed. This could be explained by the fact that the amide II band is a highly mixed mode containing contributions from the N-H in-plane bending, the C-N stretching, and the C-C stretching vibrations.⁴⁹

For more detailed analyses 2D correlation spectroscopy is used. 2D correlation spectra from temperature-dependent infrared spectra of the studied LC codendrimer on heating and on cooling were obtained. Correlation spectra clearly show the presence of synchronous and asynchronous correlation peaks among vastly different modes of molecular vibrations. In practice, when 2D correlation analyses are done, it is usually more convenient to scan only a part of the correlation map to pick up a useful local feature of the correlation intensity profile rather than displaying the entire spectral region. Therefore, the contour maps in the 3000–3600, 2800–3000, 1400–1800, and 900–1400 cm⁻¹ regions for three temperature ranges room temperature (18 °C) – 30 °C, 50–70 °C, and 95–110 °C were made.^{43,50}

Figure 8 shows synchronous (a) and asynchronous (b) correlation spectra of the LC codendrimer in the 3600–3000 cm⁻¹ region between room temperature and 30 °C. For the synchronous correlation spectrum, three autopeaks at 3425,

3254, and 3096 cm⁻¹ are found (Figure 8(a)). These indicate the significant temperature-dependent intensity of the O–H and N–H groups. The autopeak at 3425 cm⁻¹ is very broad. Thus, it seems that this autopeak consists of more than one peak. Three positive crosspeaks are observed at (3425 versus 3254 and 3096 cm⁻¹) and (3254 versus 3096 cm⁻¹) on the left up side of the synchronous correlation spectrum. These bands increase or decrease in some direction with increasing temperature.

The asynchronous correlation spectra possess excellent deconvolution ability. In the asynchronous spectrum (Figure 8b) five bands at 3452, 3405, 3329, 3204, and 3124 cm⁻¹ are identified. These bands are assigned to O–H and N–H vibrations. A pair of asynchronous peaks at 3452, 3405 cm⁻¹ may be due to a band shift, but the autopeak near 3425 cm⁻¹ is so broad that it may indicate the existence of two bands near 3425 cm⁻¹.

On the basis of the rule proposed by Noda, the intensity of bands changes in the following sequence with temperature: 3254 → 3452, 3405 → 3329 → 3124 → 3096 cm⁻¹. This sequence means that the moment of free NH groups is changing first, followed by the free and bonded OH groups and then bonded NH groups, respectively.

In the synchronous spectrum after 50 °C (Figure 8c) only two autopeaks at 3254 and 3096 cm⁻¹ and one crosspeak at 3254 versus 3096 cm⁻¹ are observed. The autopeak at 3425 cm⁻¹ disappears after this temperature. In the asynchronous spectrum (Figure 8d) the crosspeaks corresponding to five bands at 3415, 3355, 3265, 3170, and 3080 cm⁻¹ are evidenced. It can be seen that all of these bands are shifted when comparing with those acquired before, between room temperature and 30 °C. On cooling the process is reversed.

The synchronous and asynchronous correlation spectra of the 3000–2800 cm⁻¹ region are represented in Figure 9. Four autopeaks at 2847, 2917, 2938, and 2974 cm⁻¹, four positive crosspeaks at (2974 versus 2938) cm⁻¹, (2958 versus 2917 and 2847) cm⁻¹ and (2917 versus 2847) cm⁻¹, and two negative crosspeaks at (2938 versus 2917 and 2847) cm⁻¹ can be seen in the synchronous correlation spectrum recorded between room temperature and 30 °C (Figure 9a). Positive crosspeaks in the synchronous correlation spectrum indicate that the reorientation directions of transition dipole moments of two relative stretching modes are the same, while the negative crosspeaks show that the reorientation direction of one transition dipole moment is perpendicular to that of the other transition dipole moment. This means that the bands at 2974 with 2938 cm⁻¹ and at 2958 with 2917 and 2847 cm⁻¹ vary in some direction, and the bands at 2938 with 2917 and 2847 cm⁻¹ vary in opposite directions (symmetric vibration of CH₂ and CH₃ vary in opposite directions with asymmetric vibration of these groups).

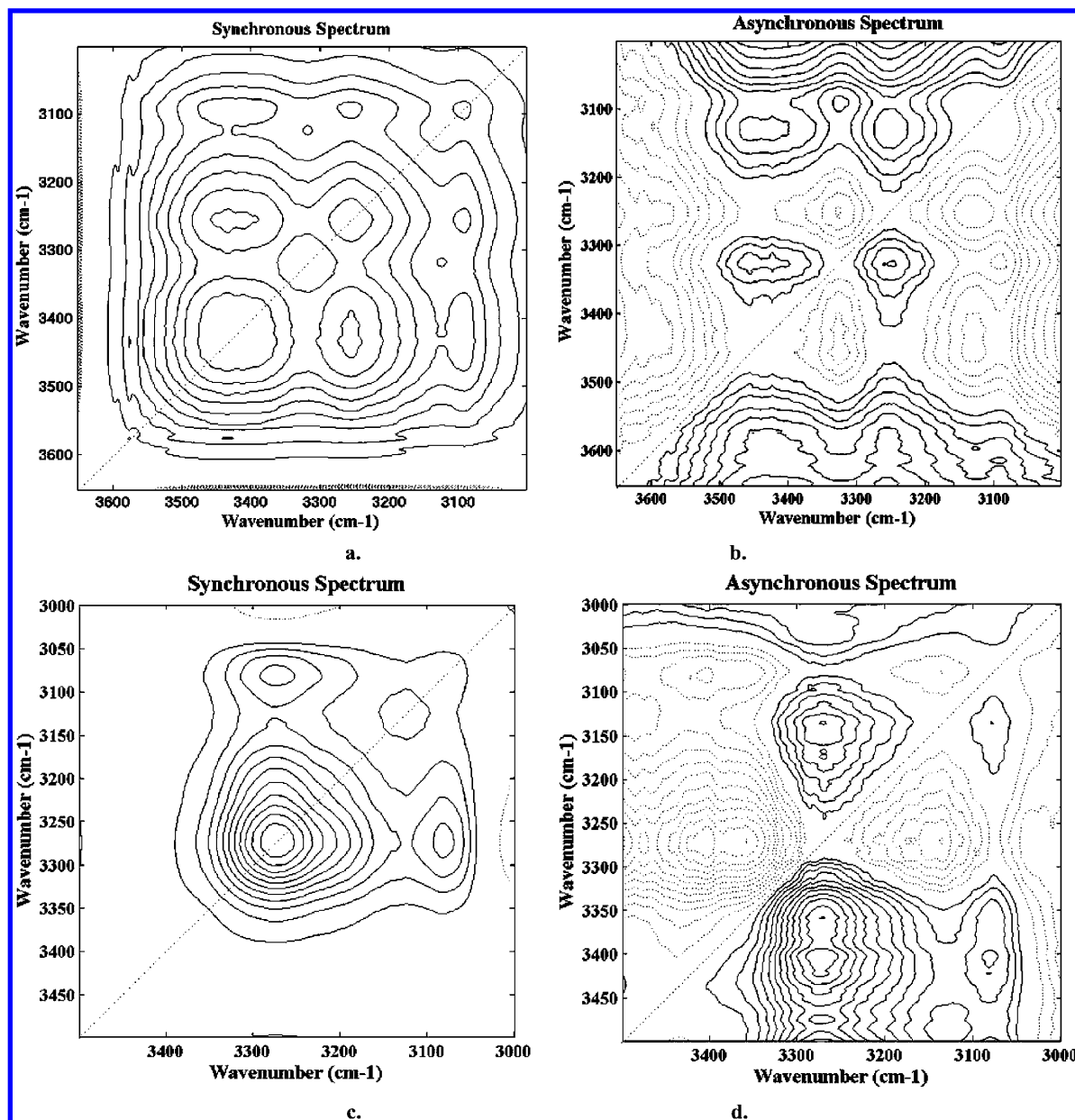


Figure 8. Synchronous and asynchronous spectra in the 3600–3000 cm^{-1} region until 30 °C (a), (b) and after 50 °C (c), (d).

In the asynchronous correlation spectrum in this region (Figure 9b) two new bands at 2958 and 2864 cm^{-1} are evidenced. The 2974 and 2958 cm^{-1} are assigned to CH_3 asymmetric stretching modes, that at 2938 can be assigned to CH_2 asymmetric stretching modes, and the bands at 2917 and 2847 cm^{-1} are due to CH_2 and CH_3 symmetric stretching modes.

On the basis of the Noda's rule, the intensity of bands changes in the following sequence with temperature: 2864 \rightarrow 2958 \rightarrow 2938 \rightarrow 2847 \rightarrow 2917 cm^{-1} . This sequence means that the CH_3 group changed its moment before CH_2 .

In the synchronous correlation spectrum between 50 and 70 °C (Figure 9c) the following peaks can be detected: four autopeaks at 2847, 2917, 2938, and 2974 cm^{-1} , two positive crosspeaks at (2974 versus 2938) and (2917 versus 2847) cm^{-1} , and four negative crosspeaks at (2974 versus 2917 and 2847) cm^{-1} and at (2938 versus 2917 and 2847) cm^{-1} . This means that the bands at 2974 with 2938 and 2917 with 2847 cm^{-1} vary in some direction, and the bands at 2974 and 2938 cm^{-1} vary in opposite direction with 2917 and 2847 cm^{-1} .

In the asynchronous correlation spectrum in this region another new band at 2884 cm^{-1} is evidenced. In this case, the

intensity of bands changes in the following sequence with temperature: 2864 \rightarrow 2958 \rightarrow 2974 \rightarrow 2938 \rightarrow 2847 \rightarrow 2917 \rightarrow 2884 cm^{-1} .

In the temperature range 95–110 °C both synchronous and asynchronous correlation spectra are identical to those acquired in 50–70 °C. Thus, we can conclude that with increasing temperature the intensity variation of CH_3 stretching modes is faster than that of the CH_2 stretching modes. On cooling the process is reversed.

The synchronous and asynchronous correlation spectra of the 3000–3700 cm^{-1} and 1700–3000 cm^{-1} evidence significant changes near the first transition. The earlier motion of the functional groups in a solid glassy conformationally disordered state when comparing to an ordered LC conformational state achieved under thermal perturbation might explain the development of the more mobile LC phase state.

The synchronous and asynchronous correlation spectra of 1450–1800 cm^{-1} are represented in Figure 10. In the synchronous correlation spectrum, between room temperature and 30 °C (Figure 10a), 8 autopeaks can be seen at 1745, 1719, 1678, 1610, 1567, 1536, 1506, and 1467 cm^{-1} , 12 positive crosspeaks

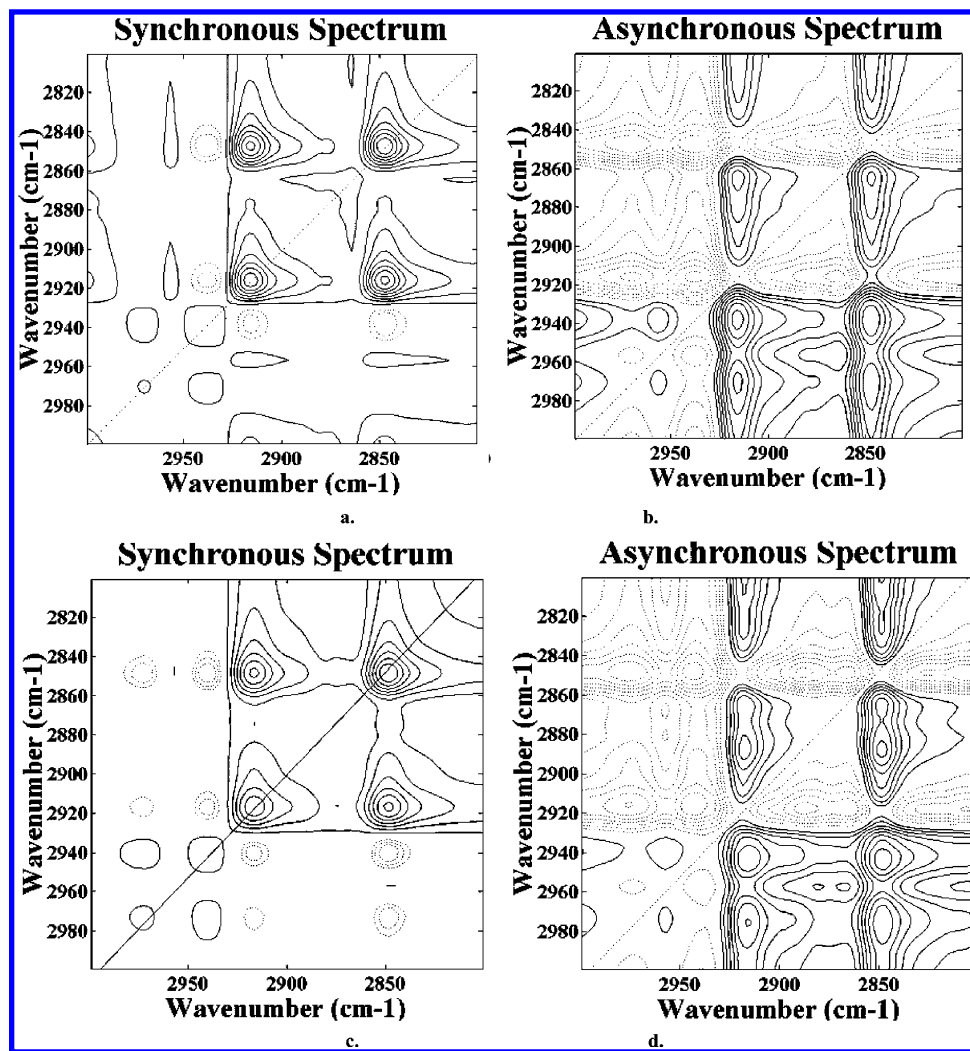


Figure 9. Synchronous and asynchronous spectra in the 2800–3000 cm^{-1} region until 30 $^{\circ}\text{C}$ (a), (b) and between 50 and 70 $^{\circ}\text{C}$ (c), (d).

at (1745 versus 1678, 1536, and 1506) cm^{-1} , (1719 versus 1610 and 1567) cm^{-1} , (1678 versus 1536 and 1506) cm^{-1} , (1610 versus 1467) cm^{-1} , (1567 versus 1467) cm^{-1} and (1536 versus 1506) cm^{-1} , and 11 negative crosspeaks at (1745 versus 1719, 1610, and 1567) cm^{-1} , (1719 versus 1678 and 1506) cm^{-1} , (1678 versus 1610 and 1567) cm^{-1} , (1610 versus 1536 and 1506) cm^{-1} , and (1567 versus 1536 and 1506) cm^{-1} . The autopeaks at 1678 and 1567 cm^{-1} show significant variations with temperature, corresponding respectively to the amide I and amide II modes.

In the synchronous correlation spectrum it can be observed that two autopeaks, one at 1745 cm^{-1} and the other at 1719 cm^{-1} , correspond to the band at 1731 cm^{-1} . The sign of the crosspeaks indicate that the temperature-dependent intensity of the C=O stretching band at 1719 cm^{-1} and the phenyl stretching band at 1610 cm^{-1} change in similar direction, while that of the C=O group stretching band at 1745 cm^{-1} and the phenyl ring stretching band change in reverse direction. As a result, the band at 1747 cm^{-1} can be assigned to the C=O group conjugated with the phenyl ring, while the band at 1719 cm^{-1} is due to the C=O near the chiral center. The splitting of the C=O stretching band indicates that there are s-trans and s-cis rotational conformers.⁴³

It can be noticed that the bands corresponding to the amide I and II modes vary in opposite directions with increasing temperature.

The asynchronous correlation spectrum in this region is shown in Figure 10b. In this spectrum six new bands are identified at 1640, 1618, 1597, 1583, 1518, and 1500 cm^{-1} . This can give us some new information as follows. The band at 1610 cm^{-1} actually splits into two bands located at 1597 cm^{-1} and 1618 cm^{-1} . These bands may originate from the two rotational conformers possible for the ester group.⁵¹ Also, the amide II vibrations are composed of two separate bands at 1583 and 1560 cm^{-1} ascribed to free NH and H-bonded NH, respectively. The band at 1675 cm^{-1} corresponding to amide I mode and the band at 1640 cm^{-1} corresponding to the vibrations of the CH=N groups are evidenced, too. The sequence of spectral intensity of these groups changing in the ascending order of temperature is given by 1675 $\text{cm}^{-1} \rightarrow 1640$ and 1560 $\text{cm}^{-1} \rightarrow 1583$ cm^{-1} .

It is worthwhile to remark here that the excellent deconvolution ability of the asynchronous correlation spectrum does not indicate any splitting behavior of the amide I band. The amide I band is a mixed mode containing a large contribution from the carbonyl stretching vibration. It is expected for the amide I mode to have infrared bands attributed to free and H-bonded carbonyl groups. Moreover it is well-known that amide I band is sensitive to ordered and disordered domains, and it appears that in our case it is not possible to have such a discrimination of the carbonyl bands. An explanation could be the presence in this region of highly overlapping bands, but this result could also be understandable for our system in which the hydrogen bonds between the amide groups have the role of preserving

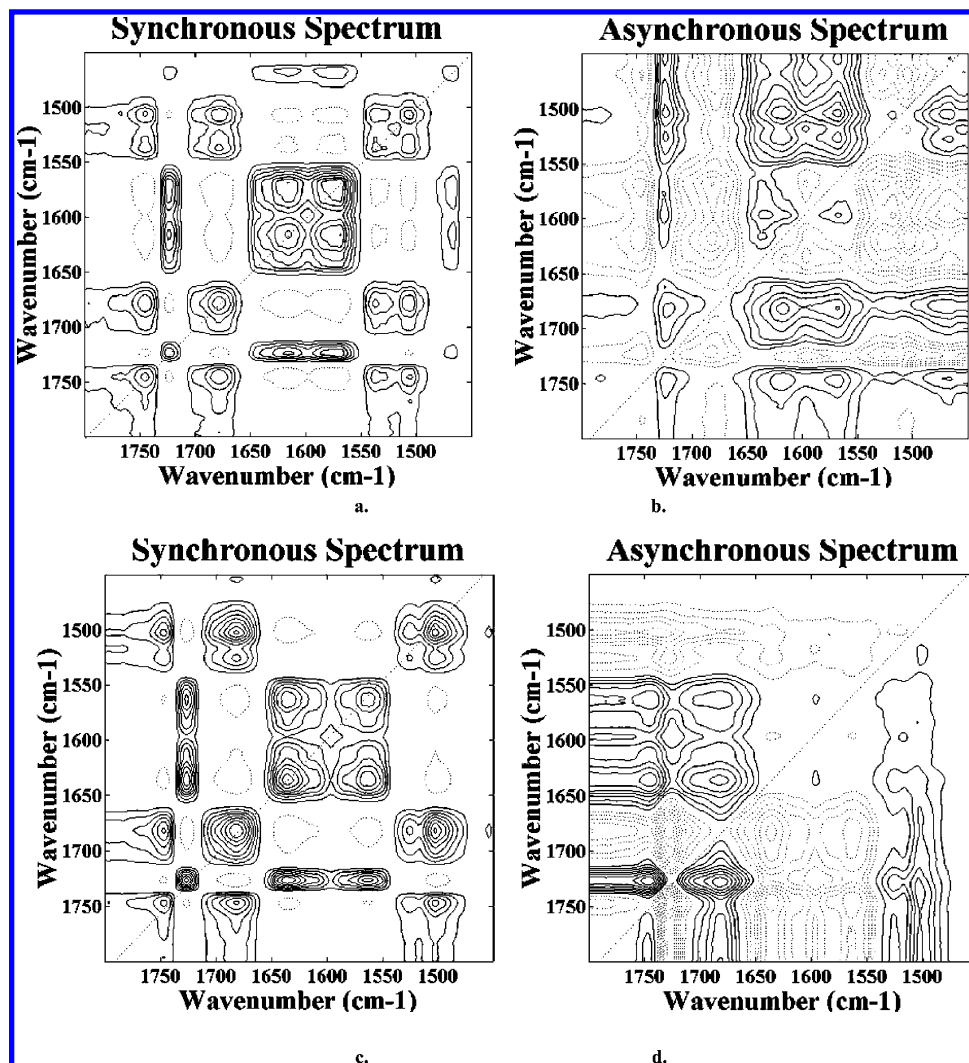


Figure 10. Synchronous and asynchronous spectra in the 1450–1800 cm^{-1} region until 30 °C (a), (b) and between 95 and 110 °C (c), (d).

the rigidity of an aggregated central dendritic structure. For our system exhibiting microphase separation driven LC phases the achieved degree of order is rather low.

In the temperature range 50–70 °C both synchronous and asynchronous correlation spectra are identical to those of the 18–30 °C temperature range.

In the synchronous correlation spectrum (Figure 10c) in the temperature range of 95–110 °C seven autopeaks at 1745, 1725, 1678, 1640, 1560, 1536, and 1506 cm^{-1} can be seen. Positive crosspeaks appear at (1745 versus 1678, 1536, and 1506) cm^{-1} , (1725 versus 1640 and 1560) cm^{-1} , (1678 versus 1536 and 1506) cm^{-1} , (1640 versus 1560) cm^{-1} , and (1536 versus 1506) cm^{-1} and negative crosspeaks at (1745 versus 1725, 1640, and 1560) cm^{-1} , (1725 versus 1678 and 1506) cm^{-1} , (1678 versus 1640 and 1560) cm^{-1} , (1640 versus 1506) cm^{-1} , and (1560 versus 1506) cm^{-1} .

In the asynchronous spectrum (Figure 10d), major changes appear associated with the structural changes which soften the central dendrimeric core resulting in a change in molecular shape. Therefore, the sequence of spectral intensity change in the ascending order of temperature is given by 1583 cm^{-1} → 1560 and 1640 cm^{-1} → 1685 cm^{-1} . The band at 1610 cm^{-1} is not split into two bands (located at 1597 and 1618 cm^{-1}) like in previous cases (temperature interval 18–30 and 50–70 °C); in this case only a band at 1597 cm^{-1} is located. The splitting is reduced due to the decreasing interaction which appeared with the increasing temperature.

In the temperature range 18–70 °C both synchronous and asynchronous spectra remained unchanged. The sequence of spectral intensity change is 1675 cm^{-1} → 1640 and 1560 cm^{-1} → 1583 cm^{-1} , i.e., amide I, azomethine, and amide II. In the temperature range 95–110 °C in which the dendrimeric scaffold is softer due to the gain in energy and consequently more easily conformational changes are allowed, the sequence of spectral intensity change is reversed: 1583 cm^{-1} → 1560 and 1640 cm^{-1} → 1685 cm^{-1} . For this spectral region the first LC transition does not lead to significant changes of the constituent bands.

The results found on cooling are similar. In the synchronous spectrum (not shown) seven autopeaks have been observed at 1745, 1725, 1678, 1640, 1610, 1560, and 1506 cm^{-1} . The intensity of the autopeak at 1530 cm^{-1} is too weak to be seen, but the corresponding crosspeaks are visible. Positive crosspeaks appear at (1745 versus 1725, 1678, 1520, and 1506) cm^{-1} , (1725 versus 1678, 1640, 1610, 1560, 1530, and 1467) cm^{-1} , (1678 versus 1530 and 1506) cm^{-1} , (1640 versus 1610, 1560, 1520, and 1467) cm^{-1} , (1610 versus 1560, 1520, and 1467) cm^{-1} , (1560 versus 1520 and 1467) cm^{-1} and (1530 versus 1506) cm^{-1} and negative crosspeaks at (1745 versus 1640 and 1560) cm^{-1} , (1678 versus 1640 and 1560) cm^{-1} , (1640 versus 1506) cm^{-1} , and (1560 versus 1506) cm^{-1} . In the synchronous spectrum the two autopeaks, one at 1745 cm^{-1} and another at 1725 cm^{-1} , are corresponding to the band at 1731 cm^{-1} . The sign of the crosspeaks indicates that temperature-dependent intensity of the ester C=O stretching band at 1725 cm^{-1} and the phenyl

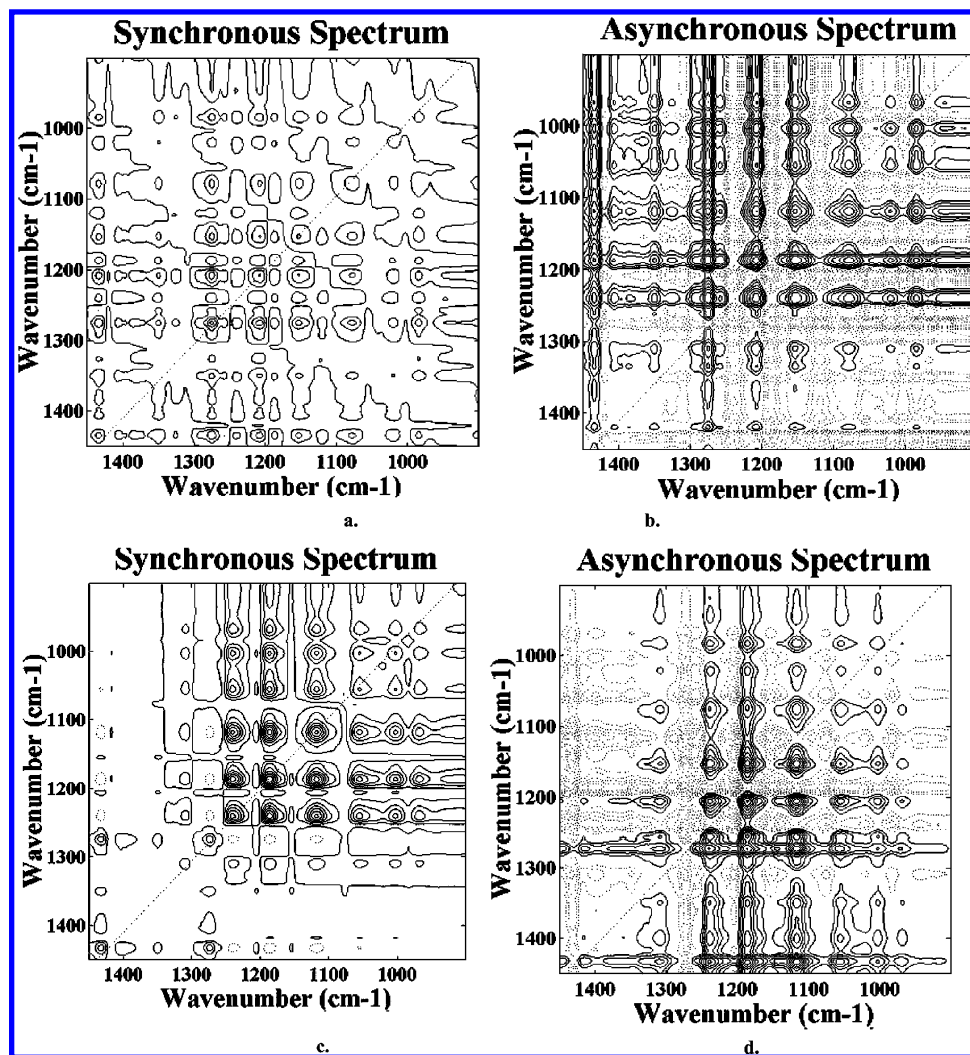


Figure 11. Synchronous and asynchronous spectra in the 900–1450 cm^{-1} region until 30 $^{\circ}\text{C}$ (a), (b) and between 50 and 70 $^{\circ}\text{C}$ (c), (d).

stretching band at 1610 cm^{-1} changes in a similar direction, while that of the C=O group stretching band at 1745 cm^{-1} and the phenyl ring stretching band changes in the reverse direction.

In the asynchronous correlation spectrum (not shown) between the 93 and 78 $^{\circ}\text{C}$ temperature region, the band at 1610 cm^{-1} is again split into two bands located at 1597 cm^{-1} and 1618 cm^{-1} . Again, amide II vibrations are composed of two separate bands at 1583 and 1560 cm^{-1} . The sequence of spectral intensity of groups changing in the descending order of temperature is given by 1675 cm^{-1} \rightarrow 1640 and 1560 cm^{-1} \rightarrow 1583 cm^{-1} . In the temperature region lying between 45 and 18 $^{\circ}\text{C}$ the sequence of spectral intensity of the amide groups changing in the descending order of temperature is reversed (1583 cm^{-1} \rightarrow 1560 and 1640 cm^{-1} \rightarrow 1675 cm^{-1}).

In the synchronous correlation spectrum, between room temperature and 30 $^{\circ}\text{C}$ (Figure 11a), in the 900–1800 region, one can observe autopeaks at 1432, 1275, 1207, 1189, 1153, 1079, 1021, and 982 cm^{-1} . All autopeaks are forming positive crosspeaks. The band at 1275 cm^{-1} corresponding to the vibrations of the C–O–C groups exhibits significant variations with temperature. Whereas it is not conclusive with the synchronous spectrum, the asynchronous spectrum (Figure 11b) provides very rich information about the two types of methyl groups present in the LC codendrimer system. The methyl asymmetric deformation band is observed at 1435 cm^{-1} and the symmetric deformation band at 1385 cm^{-1} . The band for the symmetric deformation of the methyl group at 1385 cm^{-1}

has side peaks at 1388 and 1364 cm^{-1} probably due to the sharpening of this band. The bands for the stretching deformation of C–O–C groups are identified at 1325, 1293, 1275, 1254 cm^{-1} ; the bands for symmetric deformation of $\text{CH}_2\text{--N}$ are observed at 1408, 1350, 1207, and 1153 cm^{-1} and the amide III band at 1309 cm^{-1} . The sequence of spectral intensity change in the ascending order of temperature is given by 1435 cm^{-1} \rightarrow 1275 cm^{-1} \rightarrow 1207, 1406 cm^{-1} \rightarrow 1350, 1290 cm^{-1} \rightarrow 1250 cm^{-1} \rightarrow 1325, 1388, 1364 cm^{-1} \rightarrow 1310, 1150 cm^{-1} . The intensity of the band at 1435 cm^{-1} ascribed to the asymmetric deformation of the methyl groups is the first which modifies with increasing temperature, followed by the modification of the intensity of the band at 1275 cm^{-1} corresponding to the vibrations of C–O–C groups; the variations of the other bands take place at higher temperatures.

In the synchronous spectrum of the temperature range 50–70 $^{\circ}\text{C}$ (Figure 11c), six new autopeaks appear at 1310, 1250, 1120, 1050, 1005, and 965 cm^{-1} with the vanishing of the autopeaks at 1150 and 1079 cm^{-1} . These results indicate that the intensity of the autopeaks is not changing or is slightly changing up to the first transition, but they change only after. The intensity of the bands at 1150 and 1079 cm^{-1} is modifying up to the first transition and then remains constant. Significant modifications with temperature are shown by the bands at 1275, 1250, 1188, and 1120 cm^{-1} .

Also in this case, the asynchronous spectrum is very complex (Figure 11d). The sequence of the spectral intensity change in

the ascending order of temperature in this case is given by 1435, 1275 $\text{cm}^{-1} \rightarrow$ 1406, 1370, 1350, 1290, 1207 $\text{cm}^{-1} \rightarrow$ 1153 $\text{cm}^{-1} \rightarrow$ 1330, 1310 cm^{-1} . It can be observed that the first bands which modify with increasing temperature are those corresponding to the asymmetric deformations of the methyl groups and C–O–C groups. These are followed by the symmetric deformation of the CH_2 –N, methyl, C–O–C, C–N stretching, and amide III.

Both the synchronous and asynchronous spectra in the temperature range 95–110 °C are identical to those found in 50–70 °C.

The results found on cooling in the 900–1800 cm^{-1} region are also similar as in the spectral region described above. In the synchronous spectrum (not shown) between 93 and 78 °C autopeaks are found at 1432, 1399, 1312, 1276, 1240, 1207, 1189, 1120, 1079, 1056, and 1004 cm^{-1} . All autopeaks form crosspeaks. The crosspeaks at (1432 versus 1240, 1189, and 1020) and (1276 versus 1240, 1179, and 1120) are negative and the other ones are positive. The sequence of spectral intensity change in the ascending order of temperature evidenced from the asynchronous spectrum (not shown) is given by 1275 $\text{cm}^{-1} \rightarrow$ 1207, 1156 $\text{cm}^{-1} \rightarrow$ 1435 $\text{cm}^{-1} \rightarrow$ 1412, 1348, 1364 $\text{cm}^{-1} \rightarrow$ 1310 cm^{-1} .

It can be noticed that the band corresponding to the symmetric vibrations of the methyl groups is not split in two anymore. Only a new band at 1364 cm^{-1} is noticed. On cooling the bands corresponding to the vibrations of C–O–C are the most sensitive, followed by the variations of the bands of the N–H groups, methyl, amide III.

In the synchronous spectrum in the temperature range 45–18 °C (not shown), 9 autopeaks appear at 1432, 1312, 1276, 1240, 1207, 1189, 1120, 1056, and 1005 cm^{-1} . The sign of the autopeaks is the same as in the previous case. The asynchronous spectrum is very complex (not shown). The sequence of spectral intensity change in the ascending order of temperature in this case is given by 1312 $\text{cm}^{-1} \rightarrow$ 1207, 1156, 1412 $\text{cm}^{-1} \rightarrow$ 1435 $\text{cm}^{-1} \rightarrow$ 1270 cm^{-1} .

Conclusions

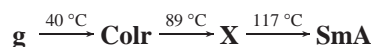
A liquid crystal poly(amidoamine) generation 3 codendrimer (PAMAM (L_1)16(L_2)16), functionalized in the terminal groups by one-chain promesogenic calamitic units ((4-(4'-decyloxybenzoyloxy)salicylaldehyde (L_1)) and two-chain promesogenic calamitic units (4-(3',4'-didecyloxybenzoyloxy)salicylaldehyde (L_2))), was investigated by FT-IR and 2D correlation spectroscopy.

The modifications occurred in the 2700–3800 cm^{-1} , 1000–1800 cm^{-1} , and 600–1000 cm^{-1} spectral regions and revealed the microstructural changes occurring on phase transitions contributed to a better understanding of the packing scheme.

The transition temperatures were determined, with good accuracy through the fitting of the integral absorption curves with Boltzmann functions.

The values of the calculated transition temperatures agree with the LC transition temperatures determined by DSC. In addition, another spectral modification with temperature not detected by DSC as a phase transition was evidenced, and it was connected with the high degree of plasticity of molecules of this type with molecular conformation rearrangements affording the change in shape of the central dendritic scaffold from prolate characteristic to a columnar structure, to oblate characteristic to a lamellar structure.

Taking into account the previously reported results of X-ray, DSC, and POM observations^{19–23} and the present spectral study the following sequence was detected:



Significant changes with temperature were obtained at the level of the OH and NH groups and amide I and amide II modes proving the important role of hydrogen bonding in the formation and stabilization of the liquid-crystalline phases: the hydrogen bonds between the amide groups preserve the rigid aggregated central dendritic structure important in stabilizing the columnar structure. With increasing temperature and H-bonding breaking, the achieved increased chain mobility and conformational freedom allows for formation of the layered structure.

Additionally, a more detailed study was carried out using 2D correlation spectroscopy. This method is particularly useful for the analysis of the highly overlapped bands and the determination of the sequential order of the intensity changes caused by an external perturbation.

Three temperature ranges on heating and two temperature ranges on cooling were investigated by this method. The 2D correlation spectra revealed significant modifications occurring around the first LC transition in the spectral regions 2700–3800 cm^{-1} and 1000–1450 cm^{-1} with vibrations of NH, OH, aliphatic, and COC groups. The 2D correlation spectra in the 1450–1800 cm^{-1} region characteristic to vibrations of amide I and II modes, ester carbonyl evidenced significant changes around 89 °C associated with molecular conformational rearrangements.

By means of 2D correlation spectroscopy the band at 1731 cm^{-1} corresponding to ester carbonyl groups was resolved into two bands: one at 1745 cm^{-1} and another at 1719 cm^{-1} . The splitting of the C=O stretching band indicates the existence of s-trans and s-cis rotational conformers.

Interestingly, the amide I band did not present any splitting behavior, even that corresponding to free and H-bonded carbonyl groups. Actually it was expected that this mode would show an enhanced splitting behavior being also sensitive to ordered and disordered domains. An explanation to this result could be the low degree of order in the studied system.

In the investigated temperature ranges the following sequences for intensity changes were found:

OH 3452, 3405 \rightarrow 3329 cm^{-1} free OH, H-bonded OH

NH 3254 \rightarrow 3124 \rightarrow 3096 cm^{-1} free NH, H-bonded NH

aliphatic 2864 \rightarrow 2958 \rightarrow 2938 \rightarrow 2847 \rightarrow
2917 cm^{-1} (CH_3 , CH_2)

amide II 1560 $\text{cm}^{-1} \rightarrow$ 1583 cm^{-1} H-bonded NH, free NH

Acknowledgment. Daniela Filip acknowledges the financial support of EU network on Super Molecular Liquid Crystal Dendrimers (RTN-LCDD) - HPRN-CT-2000-00016 and a fellowship and well as Portuguese Science Foundation (FCT) for the granted fellowship SFRH/BPD/19722/2004 and the financial support within the project POCTI/CTM/56382/2004.

References and Notes

- (1) Frechet, J. M.; Hawker, C. J.; Gitsov, I.; Leon, J. W. *Pure Appl. Chem.* **1996**, A33, 1399.
- (2) Mourey, T. H.; Turner, S. R.; Rubinshtain, M.; Frechet, J. M.; Hawker, C. J.; Wooley, K. L. *Macromolecules* **1992**, 25, 2401.

- (3) Wooley, K. L.; Hawker, C. J.; Pochan, J. M.; Frechet, J. M. *Macromolecules* **1993**, *26*, 1514.
- (4) Jansen, J. F.; de Brabader-van de Berg, E. M.; Meijer, E. W. *Science* **1994**, *266*, 1226.
- (5) Tomalia, D. A.; Durst, H. D. *Top. Curr. Chem.* **1993**, *165*, 193.
- (6) Newcome, G. R.; Moorefield, C. N.; Vogtle, F. *Dendritic molecules: concept, synthesis, perspectives*; VSH: Weinheim, 1996.
- (7) Frey, H.; Lach, C.; Lorenz, K. *Adv. Mater.* **1998**, *10*, 279.
- (8) Vogtle, F.; Plevovets, M.; Nieger, M.; Azzellini, G. C.; Credi, A.; De Cola, L.; De Marchis, V.; Venturi, M.; Balzani, V. *J. Am. Chem. Soc.* **1999**, *121*, 6290.
- (9) Adronov, A.; Malenfant, P. R.; Frechet, J. M. *Chem. Mater.* **2000**, *12*, 1463.
- (10) Weener, J. W.; Meijer, E. W. *Adv. Mater.* **2000**, *12*, 741.
- (11) Wang, J.; Jia, H.; Zhong, H.; Wu, H.; Yo, L.; Xu, H.; Li, M.; Wei, Y. *J. Polym. Sci., Part A: Polym. Chem.* **2000**, *38*, 4147.
- (12) Ponomarenko, S. A.; Boiko, N. I.; Shibaev, V. P. *Polym. Sci. C* **2001**, *43*, 1601.
- (13) Mathews, O.; Shipway, A.; Stoddart, J. *Prog. Polym. Sci.* **1998**, *23*, 1.
- (14) Beletskaya, I. P.; Chuchurjukin, A. V. *Russ. Chem. Rev.* **2000**, *69*, 639.
- (15) Baars, M. W.; Sontjns, S.; Fischer, H. M.; Pcerling, H. W.; Meijer, E. W. *Chem. Eur. J.* **1998**, *4*, 2456.
- (16) Boiko, N.; Zhu, X.; Vinokur, R.; Rebrov, E.; Muzafarov, Az.; Shibaev, V. *Ferroelectrics* **2000**, *243*, 59.
- (17) Saez, I. M.; Goodby, J. W. *Liq. Cryst.* **1999**, *26*, 1101.
- (18) Ponomarenko, S. A.; Boiko, N. I.; Rebrov, E. A.; Muzafarov, A. M.; Whitehouse, I. J.; Richardson, R. M.; Shibaev, V. P. *Macromolecules* **2000**, *33*, 5549.
- (19) Barberá, J.; Marcos, M.; Serrano, J. L. *Chem. Eur. J.* **1999**, *5*, 1834.
- (20) Marcos, M.; Giménez, R.; Serrano, J. L.; Donnio, B.; Heinrich, B.; Guillon, D. *Chem. Eur. J.* **2001**, *7*, 1006.
- (21) Donnio, B.; Barberá, J.; Giménez, R.; Guillon, D.; Marcos, M.; Serrano, J. L. *Macromolecules* **2002**, *35*, 370.
- (22) Rueff, J.-M.; Barberá, J.; Donnio, B.; Guillon, D.; Marcos, M.; Serrano, J. L. *Macromolecules* **2003**, *36*, 8368.
- (23) Marcos, M.; Giménez, R.; Serrano, J. L.; Donnio, B.; Heinrich, B.; Guillon, D. *Chem. Eur. J.* **2001**, *7*, 1006.
- (24) Bulkin, B. J. *Advanced in Infrared and Raman Spectroscopy: Vibrational Spectra of Liquid Crystals*; Heyden: Philadelphia, PA, Vol. 8, Chapter 30.
- (25) Zhang, Z. J.; Verma, A. L.; Nakashima, K.; Yoneyama, M.; Iriyama, K.; Ozaki, Y. *Thin Solid Films* **1998**, *326*.
- (26) Bumbu, G. G.; Vasile, C.; Popescu, M.-C.; Darie, H.; Chitanu, G.; Singurel, Gh.; Carpov, A. *J. Appl. Polym. Sci.* **2003**, *88*, 2585.
- (27) Popescu, M. C.; Vasile, C.; Filip, D.; Macocinschi, D.; Singurel, Gh. *J. Appl. Polym. Sci.* **2004**, *94*, 1156.
- (28) Noda, I. *Bull. Am. Phys. Soc.* **1986**, *31*, 520.
- (29) Noda, I. *Appl. Spectrosc.* **1993**, *47*, 1329.
- (30) Nakano, T.; Shimada, S.; Saitoh, R.; Noda, I. *Appl. Spectrosc.* **1993**, *47*, 1337.
- (31) Noda, I.; Liu, Y.; Ozaki, Y. *J. Phys. Chem.* **1996**, *100*, 8665.
- (32) Smeller, L.; Heremans, K. *Vib. Spectrosc.* **1999**, *19*, 375.
- (33) Ren, Y.; Shimoyama, M.; Ninomiya, T.; Matsukawa, K.; Inoue, H.; Noda, I.; Ozaki, Y. *Appl. Spectrosc.* **1999**, *53*, 919.
- (34) Ozaki, Y.; Liu, Y.; Noda, I. *Appl. Spectrosc.* **1997**, *51*, 526.
- (35) Nakano, T.; Shimada, S.; Saitoh, R.; Noda, I. *Appl. Spectrosc.* **1993**, *47*, 1337.
- (36) Muller, M.; Buchet, R.; Fringeli, U. P. *J. Phys. Chem.* **1996**, *100*, 10810.
- (37) Wang, Y.; Murayama, K.; Myojo, Y.; Tsenkova, R.; Hayashi, N.; Ozaki, Y. *J. Phys. Chem.* **1998**, *102*, 6655.
- (38) Noda, I. *Appl. Spectrosc.* **1990**, *44*, 550.
- (39) Brecl, M.; Malavasic, T. *J. Polym. Sci., Part A, Polym. Chem.* **1997**, *35*, 2871.
- (40) Fesse, N.; Mevellec, J. Y.; Brohan, L. *Mol. Cryst. Liq. Cryst.* **2000**, *352*, 283.
- (41) Gregoriou, V. G.; Rodman, S. E.; Nair, B. R.; Hammond, P. T. *J. Phys. Chem. B* **2002**, *106*, 11108.
- (42) Gregoriou, V. G.; Rodman, S. E.; Nair, B. R.; Hammond, P. T. *Macromol. Symp.* **2002**, *184*, 183.
- (43) Cheng, Y.; Wang, X.; Cheng, J.; Sun, L.; Xu, W.; Zhao, B. *Spectrochim. Acta Part A* **2005**, *61*, 905.
- (44) Shen, Y.; Chen, E.; Ye, C.; Zhang, H.; Wu, P.; Noda, I.; Zhao, Q. *J. Phys. Chem. B* **2005**, *109*, 6089.
- (45) Czarnecki, M. A. *Appl. Spectrosc.* **1998**, *52*, 1583.
- (46) Struszczyk, H. *J. Macromol. Sci.* **1986**, *A-23* (8), 973.
- (47) Pimentel, G. C.; Sederholm, C. H. *J. Chem. Phys.* **1956**, *24*, 639.
- (48) He, L.; Yin, Z.; Zhang, M. S.; Shen, Z. X.; Chen, H. F. *Appl. Spectrosc.* **1998**, *52*, 847.
- (49) Skrovanek, D. J.; Howe, S. E.; Painter P. C.; Coleman, M. M. *Macromolecules* **1985**, *18*, 1676.
- (50) Shin, H. S.; Jung, Y. M.; Chang, T.; Ozaki, Y.; Kim, S. B. *Vib. Spectrosc.* **2002**, *29*, 73.
- (51) Beaulieu, N.; Deslongchamps, P. *Can. J. Chem.* **1980**, *58*, 164.